

# Advancements in the MRI technology for identification of dentomaxillofacial pathologies

The high-resolution imaging capabilities of Magnetic Resonance Imaging (MRI) make it highly suitable for visualizing a wide range of dentomaxillofacial pathologies, including tumors, inflammatory conditions, and vascular abnormalities. This review focuses to the role of MRI in imaging head and neck pathologies, highlighting its advantages over traditional radiodiagnostics in dentistry. MRI's ability to detect periapical lesions, differentiate between various cysts and tumors, and assess the characteristics of odontogenic and non-odontogenic lesions is discussed. Special consideration is given to the differentiation of odontogenic keratocysts and ameloblastomas, as well as the evaluation of odontogenic fibromas and myxomas using dynamic contrast-enhanced MRI. Additionally, the review explores the potential of diffusion-weighted imaging (DWI) and apparent diffusion coefficient (ADC) values in distinguishing benign from malignant lesions, emphasizing the significance of these techniques in characterizing salivary gland tumors. Future advancements in MRI technology, including the application of high-field MRI and radiomics, are also considered. Radiomics, driven by artificial intelligence, offers a promising approach to extracting quantitative features from medical images, potentially enhancing the accuracy of diagnosis and prognosis in oral cancer. The review concludes by underscoring the transformative impact of MRI in dentomaxillofacial radiodiagnostics, advocating for its broader adoption in clinical practice to improve diagnostic accuracy and patient outcomes.

**Keywords:** Diffusion-weighted imaging, magnetic resonance imaging, odontogenic cysts, odontogenic tumors, radiomics

Melisa Öçbe<sup>1</sup> 

## Introduction

Computed tomography (CT) and cone-beam computed tomography (CBCT) may be inadequate for the comprehensive assessment of either the peripheral borders of intraosseous lesions, particularly in instances where there is perforation of the bone cortex, or for the radiologic evaluation of soft tissue lesions (1). In the initial stages of diagnosis and the assessment of potential differential diagnoses, the increased signal intensity on T2w of the internal structure enhances the ability to distinguish fluid-filled cystic lesions from tumoral or malignant lesions. This contrast stems from the lack of cystic fluid composition in tumors or malignant lesions with histopathological evaluation remaining the gold standard for definitive diagnosis (2, 3).

## MRI in periapical pathologies

### Periapical lesions

MRI has the capability to detect periapical lesions at an early stage with minimal bone mineral loss, owing to its sensitivity to changes in T2 relaxation time of water molecules. Periapical lesions manifest as gray or

ORCID IDs of the authors: M.Ö. 0000-0003-1609-610X

<sup>1</sup>Kocaeli Health and Technology University, Faculty of Dentistry, Department of Oral and Maxillofacial Radiology, Kocaeli, Türkiye

Corresponding Author: Melisa Öçbe

E-mail: melisa.ocbe@kocaelisaglik.edu.tr

Received: 11 March 2024

Revised: 30 April 2024

Accepted: 24 June 2024

DOI: 10.26650/eor.20241450729

white areas distinguishable from bone marrow. As the lesion extends and thins cortical bone, a thin black line appears (3, 4) (Figure 1). Adjacent to the lesion, a black area may indicate bone sclerosis. MRI enables differentiation of substances within the lesion, identifying the presence of blood, high protein, or high cellular content. Additionally, multicontrast MRI aids in distinguishing fluid-filled cavities from encapsulated cysts, facilitating the identification of cyst cores and walls and differentiation between radicular cysts and chronic apical granulomas or other solid odontogenic formations (2-4) (Figure 2, Figure 3). In a study of Juerchott *et al.* (4), differentiation between periapical cyst and granuloma was

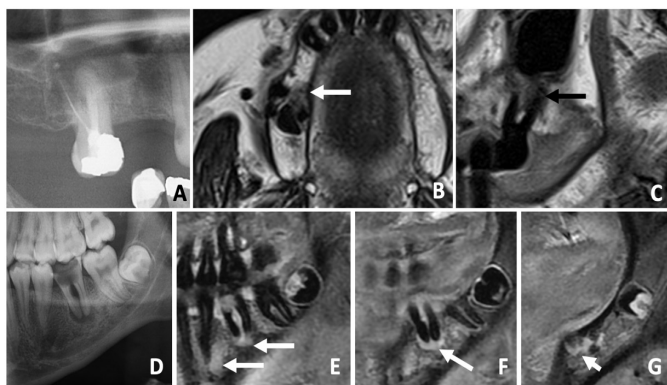


**Figure 1.** A. Panoramic radiograph showing a periapical lesion closely related to the ipsilateral maxillary sinus. B. Axial T2-weighted turbo spin echo (TSE) MRI section demonstrating low signal intensity. C. Sagittal proton density TSE MRI section displaying low signal intensity in the bone. D. Apical osteitis of the left first molar. E, F, G. Sagittal T1-weighted fat-saturated MRI sections revealing bone lesion with high signal intensity, note the caries lesion.

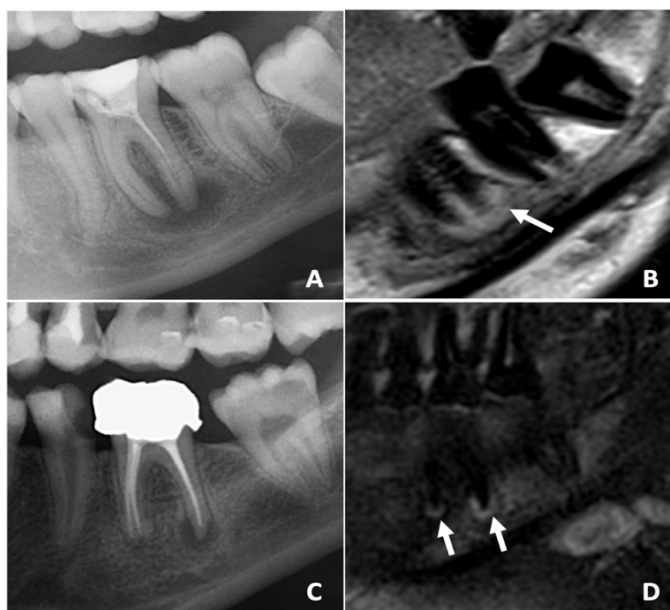


**Figure 2.** A. Cropped panoramic image depicting a periapical lesion associated with the left first molar. B. Sagittal proton density spin echo (SE) MRI section demonstrating high signal intensity. C. Cropped panoramic image revealing a periapical lesion. D. Sagittal T2-weighted spin echo (SE) MRI section displaying high signal intensity with well-defined peripheral borders.

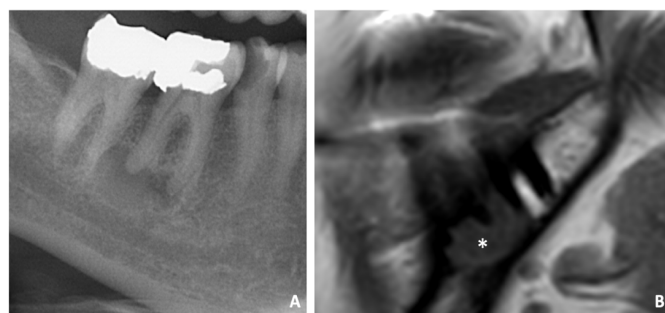


**Figure 3.** A. Cropped panoramic image displaying a radicular cyst. B. Sagittal T1-weighted MRI section demonstrating low signal intensity of the lesion (asterisk) compared to the normal bone signal intensity.

based on six characteristics: the outer margin, peripheral rim texture, lesion center texture, and involvement of surrounding tissue in contrast-enhanced T1w and T2w images, as well as the maximum thickness of the peripheral rim. Notably, cysts show well-defined margins, homogeneous textures, no surrounding tissue involvement, and a thin peripheral rim, whereas granulomas exhibit ill-defined margins, inhomogeneous textures, surrounding tissue involvement, and a thick peripheral rim (4-7).

### Differentiation of cysts and tumors with MRI

MRI plays a crucial role in the evaluation of cysts and tumors and the differential diagnosis of lesions such as ameloblastoma, odontogenic keratocyst, odontogenic or non-odontogenic cysts, nasopalatine duct cyst, or other neoplasms (5, 8-11).

#### Odontogenic fibroma and odontogenic myxoma

Specific sequences to different imaging techniques proves beneficial for a comprehensive evaluation of these lesions for preoperative assessment and treatment (5). Dynamic contrast-enhanced MRI shows potential in revealing microvessel density as an indicator of tissue activity, yet its contribution to the differential diagnosis of odontogenic tumors, except for odontogenic fibromas and myxomas, is limited (6, 7). Given the importance of preoperative discrimination between these entities, efforts have been made to identify specific MRI features for distinguishing between them. Despite similar histopathological characteristics, differences in epithelial proliferation and inflammatory reaction may provide clues for differentiation among odontogenic cysts (7).

The contrast enhancement patterns observed in dynamic contrast-enhanced MRI parameters differed between odontogenic fibroma and odontogenic myxoma, primarily in the degree of enhancement. Odontogenic fibromas exhibited higher enhancement values, particularly at 600 seconds post-contrast injection, compared to odontogenic myxomas. This distinction may be attributed to the presence of abundant myxoid or mucoid extracellular matrix in odontogenic myxomas, which is absent in odontogenic fibromas. The presence of this matrix in myxomatous tissue likely affects the inflow of contrast medium, contributing to the observed differences in contrast enhancement between the two conditions (6).

### *Odontogenic keratocyst and ameloblastoma*

Differentiating between odontogenic keratocysts and ameloblastomas with MRI involves assessing the characteristics of their cystic components (5). Studies have shown that T2 relaxation times and ADC of the cystic components can be informative in distinguishing between these two lesions. Ameloblastomas typically contain cystic components with serous liquid-containing protein, whereas odontogenic keratocyst contain desquamated keratin within their cystic components (6, 7). This difference in composition may lead to variations in T2 relaxation times and apparent diffusion coefficient (ADC) values between ameloblastomas and odontogenic keratocysts, providing valuable insights for accurate differentiation using MRI (5-8).

Unicystic ameloblastomas exhibits free diffusion and notably high ADC, likely due to the presence of less-viscous necrotic contents. Conversely, odontogenic cysts like odontogenic keratocysts and dentigerous cysts demonstrated restricted diffusion and lower ADC values, possibly attributable to increased viscosity from contents such as glycosaminoglycans and hyaluronic acid (6, 7). The signal intensity is relatively low in odontogenic keratocyst due to the presence of desquamated keratin contributes to content viscosity. The observed significant disparity in ADCs between unicystic ameloblastomas and odontogenic keratocyst suggests variations in tumor composition, emphasizing the need for additional biochemical analyses of cystic fluid (5, 7). Odontogenic keratocysts generally exhibit heterogeneous signals, with intermediate to high intensity on T1w images and intermediate intensity on T2w images (8). Regarding differentiation from ameloblastomas, odontogenic keratocysts often present with heterogeneous signals on MRI, while ameloblastomas typically display low signal intensity on T1w images and high signal intensity on T2w images. The enhancement pattern also differs, with odontogenic keratocysts showing thin enhancement of the rim on contrast-enhanced T1w images, while ameloblastomas exhibit a thicker enhancement of the rim, sometimes with papillary projections (2, 5).

### *Odontogenic keratocyst and other odontogenic cysts*

On the other hand, odontogenic cysts display homogeneous low to intermediate signal intensity on T1w images and homogeneous high signal intensity on T2w images (8). Although, it was stated that both odontogenic keratocysts and odontogenic cysts tend to exhibit an intermediate signal intensity on T1w images and a high signal intensity on T2w images. However, based solely on the signal intensity on T1w or T2w images, it is not feasible to differentiate between odontogenic keratocysts and odontogenic cysts. Instead, considering the homogeneity of signal intensity appears to hold more promise. Specifically, odontogenic keratocysts tend to display heterogeneous signal intensity, while odontogenic cysts show homogeneous signal intensity. This contrast was most evident on unenhanced T1w images (5). Regarding the contrast enhancement, it was revealed that odontogenic keratocysts and most odontogenic cysts show weak enhancement (5, 8) (Figure 4, Figure 5).

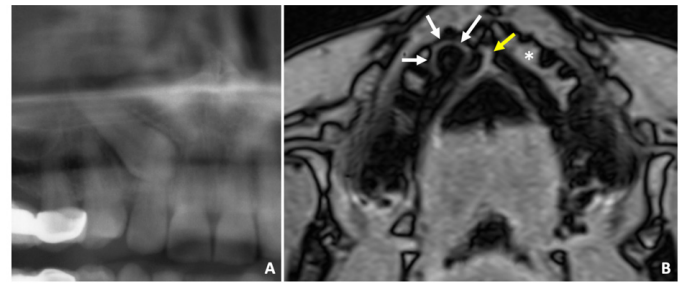


**Figure 4.** A. Cropped panoramic image displaying an impacted right canine. B. Axial T1-weighted volumetric interpolated breath-hold examination (VIBE) MRI section showing the follicle (white arrows). Please note that the internal signal intensity is lower than the normal bone signal intensity (asterisk) and the close relation with the nasopalatine canal (yellow arrow).

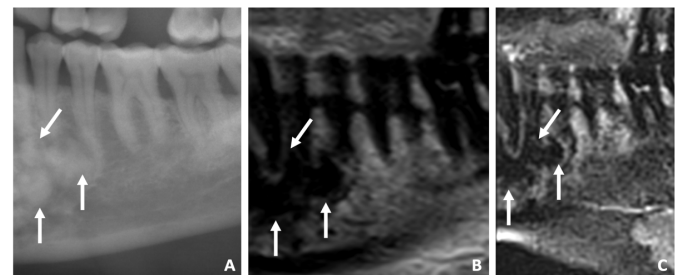


**Figure 5.** A. Cropped panoramic image displaying periapical cemental dysplasia. B. Sagittal proton density (PD) spin echo (SE) MRI section demonstrating low signal intensity of the lesion. C. Sagittal T2-weighted spin echo (SE) MRI section showing low signal intensity of the lesion.

### *Pseudocysts*

It is essential to distinguish between simple bone cysts, which are pseudocysts, and true cysts because they require different treatment approaches. However, some simple bone cysts can pose a challenge in differentiation from true cysts, especially when they appear unilocular (9). Regarding MR findings for simple bone cyst, studies have reported that T1w images typically exhibit homogeneous low or intermediate signal intensity, while T2w images show homogeneous high signal intensity. Contrast-enhanced T1w images consistently revealed enhancement of cyst walls while showing no enhancement within the cyst cavity. This differs from the MR findings observed in simple bone cysts, where contrast-enhanced T1w images depicted enhancement within the inner part of the cyst cavity. These distinctions in MR imaging indicate that simple bone cysts may be distinguishable from odontogenic cysts through contrast-enhanced T1w imaging (8). In dynamic contrast-enhanced MRI, there was found a visible progression of contrast enhancement starting from the outer edge and spreading towards the inner part of the cyst cavity over time. The time-signal intensity curves demonstrate a consistent increase in signal intensity across all cases, indicating that the contrast agent is penetrating into the cyst cavity. This ability to infiltrate into the cyst cavity distinguishes simple bone cysts from true cysts in the jaws (2, 9) (Table 1).

### *Nasopalatine Duct Cysts*

Nasopalatine duct cysts are often discovered incidentally on panoramic radiographs. Further evaluation of the lesion

**Table 1.** Comparison of MRI findings in various odontogenic lesions.

Pathology	T1-weighted (T1w)	T2-weighted (T2w)	Diffusion-weighted Imaging (DWI) - Apparent Diffusion Coefficient (ADC)	Dynamic Contrast-Enhanced MRI - Contrast Enhancement Status
Odontogenic Fibroma	Intermediate-High	Intermediate	-	Higher enhancement values, particularly at 600 seconds post-contrast injection
Odontogenic Myxoma	Intermediate-High	Intermediate -High	-	Lower enhancement values compared to odontogenic fibromas
Odontogenic Keratocyst	Intermediate- High	Heterogeneous Intermediate-High	Restricted diffusion and low ADC values	Thin enhancement of the rim contrast-enhanced T1-weighted images
Ameloblastoma	Low	High	High ADC values	Thick enhancement of the rim on contrast-enhanced T1-weighted images
Dentigerous Cyst	Low- Intermediate	High	Restricted diffusion and low ADC values	Weak enhancement
Odontogenic Cysts	Low-Intermediate	Homogeneous High	Restricted diffusion and low ADC values	Weak enhancement
Simple Bone Cyst	Homogeneous Low-Intermediate	Homogeneous High	Restricted diffusion and low ADC values	Visible progression of contrast enhancement from the margin to the inner part of the cyst cavity

requires advanced imaging techniques as CBCT or MRI. MR imaging of nasopalatine duct cyst with conventional MRI protocols were described in the literature previously (2, 10, 11) and it was stated that due to superior soft tissue contrast of MRI, even smallest soft tissue lesions can be detected. Although most of the odontogenic cysts demonstrate low signal intensity in T1w images, nasopalatine duct cyst showed high signal intensity in both T1w and T2w images (2, 11).

In case analysis of Al-Haj Hussein *et al.* (3), a specific mandibular coil was used for a dental MRI protocol. Compared to conventional MRI sequences, dental MRI provided similar results for imaging nasopalatine duct cysts. However, the authors noted that MRI features of the palate in other benign and malignant diseases typically exhibit heterogeneous signal intensity and do not display the same high signal intensity as fluids in T2w imaging, since they are not composed of cyst fluid. Therefore, in the study by Al-Haj Hussein *et al.* (3), nasopalatine duct cysts were diagnosed without intravenous contrast administration, confirming findings from previous studies (10, 11).

### Differentiation of benign and malignant lesions with MRI

#### Diffusion-weighted Imaging (DWI) and diffusion-tensor Imaging (DTI)

DWI is a technique with potential for distinguishing between benign and malignant lesions of jaws. Structural alterations within tissues, whether benign or malignant, can yield distinct signals on DWI, quantifiable through ADC values (Figure 4). These values serve as objective metrics reflecting tissue-specific diffusion capacity and have been utilized for tissue characterization and longitudinal assessments (12, 13). DTI technique involves the computation of various factors, such as mean diffusivity, degree of anisotropy, and the orientation of diffusivities. The mean diffusivity serves as a metric, shedding light on the displacement of water molecules and the presence of obstacles to their movement at

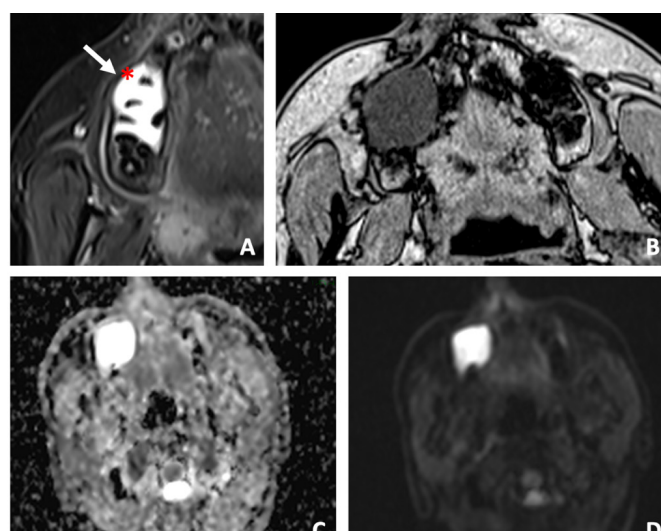


**Figure 6.** A. Radicular cyst depicted in a T2-weighted turbo spin echo (TSE) image, showing high signal intensity. Additionally, bone expansion is observed (arrow), along with destruction of the buccal bone cortex (asterisk). B. Axial T1-weighted volumetric interpolated breath-hold examination (VIBE) image displaying the lesion with low signal intensity. C. and D. Diffusion-weighted imaging (DWI) and Apparent Diffusion Coefficient (ADC) images providing information about the diffusion of water molecules within the lesion.

cellular and subcellular levels (12, 14). To extract valuable information about diffusion, DTI utilizes differently weighted DWI images. These images are processed to generate an ADC Image, which encapsulates the tissue water's diffusivity. This approach enables the characterization of microstructural features, providing a more refined and detailed representation of the underlying biological structure (7, 15-17).

#### Apparent diffusion coefficient (ADC)

The combination of ADC maps with the trace sequence is highly sensitive in detecting reduced diffusivity. In head and

neck imaging, ADC and trace diffusion imaging are increasingly utilized to evaluate benign and malignant tumors (15, 16). Generally, malignant neoplasms exhibit lower mean ADC values than benign tumors due to high cellularity, a high nuclear-to-cytoplasmic ratio, and densely packed intracellular space. Benign cystic lesions demonstrated higher ADC values compared to other lesion categories due to the increased mobility of water protons in fluid-filled cysts (7, 12, 18). However, exceptions are common, with some benign lesions showing reduced diffusivity and low mean ADC signal (i.e., abscess, Warthin tumor, schwannoma, meningioma, solitary fibrous tumor, cholesteatoma, hemangiopericytoma, myoepithelial tumor). Conversely, low-cellularity malignant tumors like chondrosarcoma and chordoma may have relatively high mean ADC values, mimicking benign lesions (12, 13).

Lymphomas exhibited lower ADC values compared to squamous cell carcinomas and adenoid cystic carcinomas. No significant difference in ADC values was observed between squamous cell carcinomas and adenoid cystic carcinomas. Inflammatory lesions showed lower ADC values compared to benign lesions but were still higher than those of malignant tumors, possibly due to differences in cellular density and secretions (13, 15, 18-22).

Conventional MRI can be utilized for the diagnosis and follow-up of osteomyelitis (23, 24); as it effectively demonstrates changes in fat tissue, abnormal bone marrow signals, and inflammatory edematous changes (25). However, MRI is prone to retaining abnormal imaging findings in the bone marrow on later follow-up scans, even when the patient's symptoms have improved. Combining MRI with functional imaging methods may address these limitations, potentially reducing the need for PET-CT as MRI techniques advance. DWI has shown promise in predicting the malignant risk of head and neck lesions, with its specificity potentially improving when combined with other functional imaging techniques (13, 17). Dynamic Contrast-Enhanced (DCE-MRI) MRI and the ADC values derived DWI have shown promise in diagnosing osteomyelitis and monitoring treatment response (23). Baba *et al.* (17) evaluated the characteristics and differences in the quantitative parameters from DCE-MRI and ADC values derived from DWI in patients before and after treatment of skull base osteomyelitis, detecting a significant decrease in ADC values post-treatment. This approach is valuable for quantifying MRI parameters for a detailed evaluation.

## **MR imaging of salivary gland tumors**

### *Signal intensity*

Salivary gland MR imaging is indicated for neoplasms rather than obstructive or inflammatory conditions. Most parotid lesions are clearly visible on T1w images due to the gland's hyperintense (fatty) background. On fat-saturated images, the bone marrow and cortex of the mandible, maxilla, and skull base appear hypointense. Enhancing (hyperintense) tissue within this hypointense background suggests bone invasion. T1w images effectively show deep infiltration into the parapharyngeal space, muscles, and bone, which strongly indicates malignancy or capsule rupture in pleomorphic adenoma (26-28).

It is commonly known that a hyperintense mass on T2w images typically indicates a benign condition, whereas a mass with low to intermediate signal intensity suggests malignancy. However, the most common benign tumor of the salivary glands, pleomorphic adenoma, exhibits very high signal intensity on T2w images (29). Despite malignant lesions typically showing low signal intensity on T2w images, exceptions include low-grade mucoepidermoid carcinoma, some adenoid cystic carcinomas, and adenocarcinomas. Additionally, Warthin tumor, although benign, can present with low or mixed signal intensity on T2w images (28, 30).

### *DWI-MRI characterization of salivary gland tumors*

Many studies have highlighted the utility of DWI in the diagnosis, staging, and monitoring of salivary gland tumors (15, 21, 27). While conventional MRI can be challenging in distinguishing between benign and malignant salivary gland tumors due to overlapping signal characteristics and enhancement patterns (26), DWI emerges as a promising technique. Recent research has demonstrated DWI's effectiveness in differentiating between benign and malignant salivary gland pathologies (27, 28, 31, 32). Milad *et al.* (27) found that ADC values for malignant salivary gland tumors were significantly lower. In the study of Assili *et al.* (31), DCE-MRI can identify tumor angiogenesis and DWI is a useful method to determine the cellularity of salivary gland tumors. However, DCE-MRI and DWI cannot be used alone for reliable differentiation of tumor types, as they may produce inaccurate results (32-34).

## **Future aspects in dentomaxillofacial radiodiagnostics**

### *Radiomics applications*

Advancements in artificial intelligence (AI) have revolutionized the interpretation of medical image data, moving from qualitative assessment to quantifiable and reproducible analysis. AI, fundamental to radiomics, plays a crucial role in extracting and selecting quantitative features from medical images. Radiomics models, driven by biomarkers, offer potential support for detailed image analysis (23, 35).

Radiomics can utilize various software tools and platforms for feature extraction, analysis, and model development. These software tools require medical images, such as MRI, CT, PET, or other modalities, as input data. The images are typically preprocessed to ensure standardized acquisition parameters and image quality before feature extraction. Once the features are extracted, they can be analyzed using statistical methods or machine learning algorithms (35, 36).

Radiomics applications in oral cancer have demonstrated significant potential for assessing tumor characteristics and predicting patient outcomes (36). Radiomics studies on ADC maps to differentiate the degree of differentiation in squamous cell carcinoma (SCC) revealed that radiomics features served as independent indicators for survival rates (37-39). These findings underscore the utility of radiomics in oral cancer management, offering valuable insights into tumor biology and prognosis (38, 39).

In a retrospective study by Bae *et al.* (40), MR images of patients with SCC and lymphoma were evaluated. Following

the segmentation of the tumors, radiomics features were extracted from both T1w and T2w images. This study demonstrates that radiomics applications can effectively differentiate SCC from lymphoma. Additionally, a study by Lu *et al.* (41) showed that combining radiomic features with clinical findings can predict lymph node metastasis. Radiomics applications hold promise for predicting not only pre-diagnosis and metastasis (40, 41) but also recurrence (42).

While the current studies (40-42) provide promising evidence for the potential of radiomics in differentiating tumor types and predicting metastasis and recurrence, there are limitations and challenges that need to be addressed. Reproducibility of radiomics features across different imaging protocols and devices needs further investigation to ensure consistency and reliability. In addition, current studies do not adequately consider the impact of tumor heterogeneity on the accuracy of radiomics predictions, which could lead to variability in results. The integration of radiomics into clinical practice requires standardization and validation across larger, more diverse patient populations to ensure its applicability and effectiveness. Future research should focus on addressing these gaps, including the development of robust algorithms that can handle diverse imaging data and the establishment of standardized protocols for radiomics feature extraction and analysis.

### High-field MRI

The potential of high-field MRI applications is promising for future advancements in MRI technology. Increased MRI resolution often leads to a compromise in signal-to-noise ratio (SNR) and tissue contrast, especially in the case of widely used 3 Tesla MRI scanners. However, ultra-high magnetic field strengths, such as in 7 Tesla MRI, offer the potential for enhanced resolution with improved tissue contrast and SNR (43, 44).

Susceptibility-weighted Imaging (SWI) MRI is a common sequence for cranial or central nervous system imaging due to its sensitivity to paramagnetic compounds (such as deoxygenated blood and iron, which lead to the distortion of the local magnetic field) is common (45). Currently, 7T SWI MRI has demonstrated efficacy in various neurological conditions including multiple sclerosis, cerebrovascular diseases, mesial temporal lobe epilepsy, cortical developmental malformations, brain tumors, and Cushing's disease. These successful outcomes underscore its potential utility in the evaluation of pathologies within the head and neck region (46, 47).

### Conclusion

In conclusion, the utilization of MRI in imaging head and neck pathologies and its extended applications beyond traditional radiodiagnostics represent a significant advancement. The high-resolution imaging capabilities and exquisite soft tissue contrast offered by MRI have revolutionized the diagnostic approach to dentomaxillofacial pathologies, enabling clinicians to accurately detect, characterize, and manage a wide range of conditions.

**Türkçe öz:** Dentomaksillofasiyal Patolojilerin Değerlendirilmesinde MRG Teknolojisindeki Gelişmeler. Manyetik Rezonans Görüntüleme (MRG), yüksek çözünürlüklü görüntüleme yetenekleri sayesinde tümörler, enflamatuvar durumlar ve vasküler anormallikler de dahil

olmak üzere geniş bir yelpazede dentomaksillofasiyal patolojilerin görüntülenmesi için son derece uygundur. Bu derleme, MRG'nin baş ve boyun patolojilerini görüntüleme rolünü incelemekte ve diş hekimliğinde geleneksel radyodiagnostiğe göre avantajlarını vurgulamaktadır. MRG'nin periapikal lezyonları tespit etme, çeşitli kistler ve tümörler arasında ayırım yapma ve odontojenik ve non-odontojenik lezyonların özelliklerini değerlendirme yeteneği ele alınmaktadır. Odontojenik keratokistler ile ameloblastomların ayırımı ve dinamik kontrastlı MRG kullanılarak odontojenik fibromlar ve miksomaların değerlendirilmesine özel bir vurgu yapılmaktadır. Ayrıca, difüzyon ağırlıklı görüntüleme (DWI) ve görünür difüzyon katsayısı (ADC) değerlerinin benign ve malign lezyonları ayırt etmedeki potansiyeli, tükürük bezi tümörlerinin karakterizasyonunda bu tekniklerin önemi vurgulanmaktadır. Gelecekteki MRG teknolojisi gelişmeleri, yüksek alanlı MRG ve radyomiks uygulamaları da ele alınmaktadır. Yapay zeka tarafından yönlendirilen radyomiks, tıbbi görüntülerden nicel özellikler çıkarmada umut verici bir yaklaşım sunmakta ve oral kanserde teşhis ve prognoz doğruluğunu artırma potansiyeline sahiptir. Derleme, MRG'nin dentomaksillofasiyal radyodiagnostikteki dönüştürücü etkisini vurgulayarak, teşhis doğruluğunu ve hasta sonuçlarını iyileştirmek için klinik pratikte daha geniş bir şekilde benimsenmesini savunarak son bulmaktadır. Anahtar Kelimeler: Difüzyon ağırlıklı görüntüleme, manyetik rezonans görüntüleme, odontojenik kistler, odontojenik tümörler, radyomiks

**Ethics Committee Approval:** Not required.

**Informed Consent:** Not required.

**Peer-review:** Due to the invited nature of this review, the manuscript did not undergo standard peer review process. Instead, it was evaluated by the dentomaxillofacial radiology section editor, Prof. Dr. Alper Sinanoğlu, to ensure its quality and relevance. The section editor provided detailed feedback to the author, and subsequent revisions were made to enhance the manuscript's clarity and scientific rigor.

**Author contributions:** MO participated in designing the study. MO participated in generating the data for the study. MO participated in gathering the data for the study. MO participated in the analysis of the data. MO wrote the majority of the original draft of the paper. MO participated in writing the paper. MO has had access to all of the raw data of the study. MO has reviewed the pertinent raw data on which the results and conclusions of this study are based. MO have approved the final version of this paper. MO guarantees that all individuals who meet the Journal's authorship criteria are included as authors of this paper.

**Conflict of Interest:** The author declared that they have no conflict of interest.

**Financial Disclosure:** The author declared that they have received no financial support.

### References

1. Kiljunen T, Kaasalainen T, Suomalainen A, Kortensniemi M. Dental cone beam CT: A review. *Phys Med* 2015;31:844-60. doi: 10.1016/j.ejmp.2015.09.004. [CrossRef]
2. Hisatomi M, Asaumi J, Konouchi H, Shigehara H, Yanagi Y, Kishi K. MR imaging of epithelial cysts of the oral and maxillofacial region. *Eur J Radiol* 2003;48:178-82. doi: 10.1016/S0720-048X(02)00218-8. [CrossRef]
3. Al-Haj Husain A, Schönegg D, Valdec S, Stadlinger B, Piccirelli M, Winklhofer S. Appearance of nasopalatine duct cysts on dental magnetic resonance imaging using a mandibular coil: Two case reports with a literature review. *Imaging Sci Dent* 2023;53:161-8. doi: 10.5624/isd.20220215. [CrossRef]
4. Juerchott A, Pfefferle T, Flechtenmacher C, Mente J, Bendszus M, Heiland S, Hilgenfeld T. Differentiation of periapical granulomas

- and cysts by using dental MRI: a pilot study. *Int J Oral Sci* 2018;10:17. doi: 10.1038/s41368-018-0017-y. [\[CrossRef\]](#)
5. Probst FA, Probst M, Pautke Ch, Kaltsi E, Otto S, Schiel S, Troeltzsch M, Ehrenfeld M, Cornelius CP, Müller-Lisse UG. Magnetic resonance imaging: a useful tool to distinguish between keratocystic odontogenic tumours and odontogenic cysts. *Br J Oral Maxillofac Surg* 2015;53:217-22. doi: 10.1016/j.bjoms.2014.10.014 [\[CrossRef\]](#)
  6. Fujita M, Matsuzaki H, Yanagi Y, Hara M, Katase N, Hisatomi M, Unetsubo T, Konouchi H, Nagatsuka H, Asaumi JI. Diagnostic value of MRI for odontogenic tumours. *Dentomaxillofac Radiol* 2013;42:20120265. doi: 10.1259/dmfr.20120265. [\[CrossRef\]](#)
  7. Han Y, Fan X, Su L, Wang Z. Diffusion-Weighted MR Imaging of Unicystic Odontogenic Tumors for Differentiation of Unicystic Ameloblastomas from Keratocystic Odontogenic Tumors. *Korean J Radiol* 2018;19:79-84. doi: 10.3348/kjr.2018.19.1.79. [\[CrossRef\]](#)
  8. Minami M, Kaneda T, Ozawa K, Yamamoto H, Itai Y, Ozawa M, Yoshikawa K, Sasaki Y. Cystic lesions of the maxillomandibular region: MR imaging distinction of odontogenic keratocysts and ameloblastomas from other cysts. *AJR Am J Roentgenol* 1996;166:943-9. doi: 10.2214/ajr.166.4.8610578. [\[CrossRef\]](#)
  9. Yanagi Y, Asaumi J, Unetsubo T, Ashida M, Takenobu T, Hisatomi M, Matsuzaki H, Konouchi H, Katase N, Nagatsuka H. Usefulness of MRI and dynamic contrast-enhanced MRI for differential diagnosis of simple bone cysts from true cysts in the jaw. *Oral Surg Oral Med Oral Pathol Oral Radiol Endod* 2010;110:364-9. doi: 10.1016/j.tripleo.2010.05.001. [\[CrossRef\]](#)
  10. Spinelli HM, Isenberg JS, O'Brien M. Nasopalatine duct cysts and the role of magnetic resonance imaging. *J Craniofac Surg* 1994;5:57-60. doi: 10.1097/00001665-199402000-00013. [\[CrossRef\]](#)
  11. Hisatomi M, Asaumi J, Konouchi H, Matsuzaki H, Kishi K. MR imaging of nasopalatine duct cysts. *Eur J Radiol* 2001;39:73-6. doi: 10.1016/s0720-048x(01)00279-0. [\[CrossRef\]](#)
  12. Grover VP, Tognarelli JM, Crossey MM, Cox IJ, Taylor-Robinson SD, McPhail MJ. Magnetic Resonance Imaging: Principles and Techniques: Lessons for Clinicians. *J Clin Exp Hepatol* 2015;5:246-55. doi: 10.1016/j.jceh.2015.08.001. [\[CrossRef\]](#)
  13. El-Gerby KM, El-Anwar MW. Differentiating Benign from Malignant Sinonasal Lesions: Feasibility of Diffusion Weighted MRI. *Int Arch Otorhinolaryngol* 2017;21:358-65. doi: 10.1055/s-0036-1597323. [\[CrossRef\]](#)
  14. Koontz NA, Wiggins RH 3rd. Differentiation of Benign and Malignant Head and Neck Lesions With Diffusion Tensor Imaging and DWI. *AJR Am J Roentgenol* 2017;208:1110-15. doi: 10.2214/AJR.16.16486. [\[CrossRef\]](#)
  15. Panyaping T, Tepkidakarn N, Kiatthanabumrung S, Wattanatranon D, Tritanon O. Usefulness of apparent diffusion coefficient values for distinguishing between squamous cell carcinoma and malignant salivary gland tumor of the head and neck. *Neuroradiol J* 2023;36:548-54. doi: 10.1177/19714009231163561. [\[CrossRef\]](#)
  16. Bao D, Zhao Y, Wu W, Zhong H, Yuan M, Li L, Lin M, Zhao X, Luo D. Added value of histogram analysis of ADC in predicting radiation-induced temporal lobe injury of patients with nasopharyngeal carcinoma treated by intensity-modulated radiotherapy. *Insights Imaging* 2022;13:197. doi: 10.1186/s13244-022-01338-w. [\[CrossRef\]](#)
  17. Baba A, Kurokawa R, Kurokawa M, Srinivasan A. Dynamic contrast-enhanced MRI parameters and apparent diffusion coefficient as treatment response markers of skull base osteomyelitis: a preliminary study. *Pol J Radiol* 2023;88:319-24. doi: 10.5114/pjr.2023.130383. [\[CrossRef\]](#)
  18. Norris CD, Quick SE, Parker JG, Koontz NA. Diffusion MR Imaging in the Head and Neck: Principles and Applications. *Neuroimaging Clin N Am* 2020;30:261-82. doi: 10.1016/j.nic.2020.04.001. [\[CrossRef\]](#)
  19. Li S, Cheng J, Zhang Y, Zhang Z. Differentiation of benign and malignant lesions of the tongue by using diffusion-weighted MRI at 3.0T. *Dentomaxillofac Radiol* 2015;44:20140325. doi: 10.1259/dmfr.20140325. [\[CrossRef\]](#)
  20. Vidiri A, Minosse S, Piludu F, Curione D, Pichi B, Spriano G, Marzi S. Feasibility study of reduced field of view diffusion-weighted magnetic resonance imaging in head and neck tumors. *Acta Radiol* 2017;58:292-300. doi: 10.1177/0284185116652014. [\[CrossRef\]](#)
  21. Zheng N, Li R, Liu W, Shao S, Jiang S. The diagnostic value of combining conventional, diffusion-weighted imaging and dynamic contrast-enhanced MRI for salivary gland tumors. *Br J Radiol* 2018;91:20170707. doi: 10.1259/bjr.20170707. [\[CrossRef\]](#)
  22. Yuan Y, Tang W, Jiang M, Tao X. Palatal lesions: discriminative value of conventional MRI and diffusion weighted imaging. *Br J Radiol* 2016;89:20150911. doi: 10.1259/bjr.20150911. [\[CrossRef\]](#)
  23. Baba A, Kurokawa R, Kurokawa M, Ota Y, Srinivasan A. Dynamic Contrast-Enhanced MRI Parameters and Normalized ADC Values Could Aid Differentiation of Skull Base Osteomyelitis from Nasopharyngeal Cancer. *AJNR Am J Neuroradiol* 2023;44:74-8. doi: 10.3174/ajnr.A7740. [\[CrossRef\]](#)
  24. Auinger AB, Dahm V, Stanisz I, Schwarz-Nemec U, Arnoldner C. The challenging diagnosis and follow-up of skull base osteomyelitis in clinical practice. *Eur Arch Otorhinolaryngol* 2021;278:4681-8. doi: 10.1007/s00405-020-06576-6. Epub 2021 Jan 28. [\[CrossRef\]](#)
  25. Clark MP, Pretorius PM, Byren I, Milford CA. Central or atypical skull base osteomyelitis: diagnosis and treatment. *Skull Base* 2009;19:247-54. doi: 10.1055/s-0028-1115325. [\[CrossRef\]](#)
  26. Yousem DM, Kraut MA, Chalian AA. Major salivary gland imaging. *Radiology*. 2000;216:19-29. doi: 10.1148/radiology.216.1.r00jl4519. [\[CrossRef\]](#)
  27. Milad P, Elbegiermy M, Shokry T, Mahmoud H, Kamal I, Taha MS, Keriakos N. The added value of pretreatment DW MRI in characterization of salivary glands pathologies. *Am J Otolaryngol* 2017;38:13-20. doi: 10.1016/j.amjoto.2016.09.002. [\[CrossRef\]](#)
  28. Habermann CR, Gossrau P, Graessner J, Arndt C, Cramer MC, Reitmeier F, Jaehne M, Adam G. Diffusion-weighted echo-planar MRI: a valuable tool for differentiating primary parotid gland tumors? *Rofo* 2005;177:940-5. doi: 10.1055/s-2005-858297. Erratum in: *Rofo*. 2005 Sep;177(9):1312. [\[CrossRef\]](#)
  29. Swartz JD, Rothman MI, Marlowe FI, Berger AS. MR imaging of parotid mass lesions: attempts at histopathologic differentiation. *J Comput Assist Tomogr* 1989;13:789-96. doi: 10.1097/00004728-198909000-00007. [\[CrossRef\]](#)
  30. Som PM, Biller HF. High-grade malignancies of the parotid gland: identification with MR imaging. *Radiology* 1989;173:823-6. doi: 10.1148/radiology.173.3.2813793. [\[CrossRef\]](#)
  31. Assili S, Fathi Kazerooni A, Aghaghazvini L, Saligheh Rad HR, Pirayesh Islamian J. Dynamic Contrast Magnetic Resonance Imaging (DCE-MRI) and Diffusion Weighted MR Imaging (DWI) for Differentiation between Benign and Malignant Salivary Gland Tumors. *J Biomed Phys Eng* 2015;5:157-68.
  32. Yabuuchi H, Kamitani T, Sagiyama K, Yamasaki Y, Hida T, Matsuura Y, Hino T, Murayama Y, Yasumatsu R, Yamamoto H. Characterization of parotid gland tumors: added value of permeability MR imaging to DWI and DCE-MRI. *Eur Radiol* 2020;30:6402-12. doi: 10.1007/s00330-020-07004-3. [\[CrossRef\]](#)
  33. Yabuuchi H, Fukuya T, Tajima T, Hachitanda Y, Tomita K, Koga M. Salivary gland tumors: diagnostic value of gadolinium-enhanced dynamic MR imaging with histopathologic correlation. *Radiology* 2003;226:345-54. doi: 10.1148/radiol.2262011486. Erratum in: *Radiology*. 2003;227(3):909. [\[CrossRef\]](#)
  34. Eida S, Sumi M, Nakamura T. Multiparametric magnetic resonance imaging for the differentiation between benign and malignant salivary gland tumors. *J Magn Reson Imaging* 2010;31:673-9. doi: 10.1002/jmri.22091. [\[CrossRef\]](#)
  35. Zhu X, Shao L, Liu Z, Liu Z, He J, Liu J, Ping H, Lu J. MRI-derived radiomics models for diagnosis, aggressiveness, and prognosis evaluation in prostate cancer. *J Zhejiang Univ Sci B* 2023;24:663-81. doi: 10.1631/jzus.B2200619. [\[CrossRef\]](#)

36. Liu S, Zhang A, Xiong J, Su X, Zhou Y, Li Y, Zhang Z, Li Z, Liu F. The application of radiomics machine learning models based on multimodal MRI with different sequence combinations in predicting cervical lymph node metastasis in oral tongue squamous cell carcinoma patients. *Head Neck* 2024;46:513-27. doi: 10.1002/hed.27605. [\[CrossRef\]](#)
37. Mossinelli C, Tagliabue M, Ruju F, Cammarata G, Volpe S, Raimondi S, Zaffaroni M, Isaksson JL, Garibaldi C, Cremonesi M, Corso F, Gaeta A, Emili I, Zorzi S, Alterio D, Marvaso G, Pepa M, De Fiori E, Maffini F, Preda L, Benazzo M, Jereczek-Fossa BA, Ansarin M. The role of radiomics in tongue cancer: A new tool for prognosis prediction. *Head Neck* 2023;45:849-61. doi: 10.1002/hed.27299. [\[CrossRef\]](#)
38. Chen J, Lu S, Mao Y, Tan L, Li G, Gao Y, Tan P, Huang D, Zhang X, Qiu Y, Liu Y. An MRI-based radiomics-clinical nomogram for the overall survival prediction in patients with hypopharyngeal squamous cell carcinoma: a multi-cohort study. *Eur Radiol* 2022;32:1548-57. doi: 10.1007/s00330-021-08292-z. [\[CrossRef\]](#)
39. Bseiso A, Saqib M, Saigol MS, Rehman A, Sare A, Yagoub AE, Mumtaz H. Patient survival prediction in locally advanced cervical squamous cell carcinoma using MRI-based radiomics: retrospective cohort study. *Ann Med Surg (Lond)* 2023;85:5328-36. doi: 10.1097/MS9.0000000000001288. [\[CrossRef\]](#)
40. Bae S, Choi YS, Sohn B, Ahn SS, Lee SK, Yang J, Kim J. Squamous Cell Carcinoma and Lymphoma of the Oropharynx: Differentiation Using a Radiomics Approach. *Yonsei Med J* 2020;61:895-900. doi: 10.3349/ymj.2020.61.10.895. [\[CrossRef\]](#)
41. Lu S, Ling H, Chen J, Tan L, Gao Y, Li H, Tan P, Huang D, Zhang X, Liu Y, Mao Y, Qiu Y. MRI-based radiomics analysis for preoperative evaluation of lymph node metastasis in hypopharyngeal squamous cell carcinoma. *Front Oncol* 2022;12:936040. doi: 10.3389/fonc.2022.936040. [\[CrossRef\]](#)
42. Caprini E, D'Agnes G, Brennan PA, Rahimi S. Human papillomavirus-related oropharyngeal squamous cell carcinoma and radiomics: A new era? *J Oral Pathol Med* 2023;52:300-4. doi: 10.1111/jop.13419. [\[CrossRef\]](#)
43. Chen X, Qu L, Xie Y, Ahmad S, Yap PT. A paired dataset of T1- and T2-weighted MRI at 3 Tesla and 7 Tesla. *Sci Data* 2023;10:489. doi: 10.1038/s41597-023-02400-y. [\[CrossRef\]](#)
44. Trattinig S, Springer E, Bogner W, Hangel G, Strasser B, Dymerska B, Cardoso PL, Robinson SD. Key clinical benefits of neuroimaging at 7T. *Neuroimage* 2018;168:477-89. doi: 10.1016/j.neuroimage.2016.11.031. [\[CrossRef\]](#)
45. Clarke MA, Witt AA, Robison RK, Fleishman S, Combes AJE, Houston D, Prock LE, Sweeney G, O'Grady KP, McKnight CD, Smith SA. Cervical spinal cord susceptibility-weighted MRI at 7T: Application to multiple sclerosis. *Neuroimage* 2023;284:120460. doi: 10.1016/j.neuroimage.2023.120460. [\[CrossRef\]](#)
46. de Rotte AA, Groenewegen A, Rutgers DR, Witkamp T, Zelissen PM, Meijer FJ, van Lindert EJ, Hermus A, Luijten PR, Hendrikse J. High resolution pituitary gland MRI at 7.0 tesla: a clinical evaluation in Cushing's disease. *Eur Radiol* 2016;26:271-7. doi: 10.1007/s00330-015-3809-x. [\[CrossRef\]](#)
47. Bonacchi R, Pagani E, Meani A, Cacciaguerra L, Preziosa P, De Meo E, Filippi M, Rocca MA. Clinical Relevance of Multiparametric MRI Assessment of Cervical Cord Damage in Multiple Sclerosis. *Radiology* 2020;296:605-15. doi: 10.1148/radiol.2020200430. [\[CrossRef\]](#)